doi: 10.3969/j.issn.1673-9736.2016.03.04
Article ID: 1673-9736(2016)03-0153-11

Geochronology, geochemistry and Hf isotope of monzogranite in Niubiziliang of Qinghai

JIANG Hefang[1], SUN Fengyue[1], LI Liang[1], LI Ruihua[2,3], YU Lu[1], WANG Fei[1] and SHEN Dali[4]

1. *College of Earth Sciences, Jilin University, Changchun 130061, China;*
2. *MLR Key Laboratory of Metallogeny and Mineral Resources Assessment, Institute of Mineral Resources, Chinese Academy of Geological Sciences, Beijing 100037, China;*
3. *School of Earth and Space Sciences, Perking University, Beijing 100871, China;*
4. *Qinghai Nuclear Industrial Geology Bureau, Xining 810008, China*

Abstract: Zircon U-Pb dating, whole-rock geochemical analyses and Hf isotope are undertaken for the monzogranite in Niubiziliang area with the aim of constraining its formation time, petrogenesis and the regional tectonic setting. The zircons from monzogranite are euhedral-subhedral in shape, and display rhythm growth zoning, indicating a magmatic origin. LA-ICP-MS zircon U-Pb dating indicates the monzogranite formed most probably in the Late Devonian (359.0±2.6 Ma). The monzogranite has SiO_2 = 74.69%-76.11%, Al_2O_3 = 12.07%-12.81%, $Na_2O + K_2O$ = 8.24%-8.70%, Na_2O/K_2O = 0.60-0.68, A/CNK > 1, which shows that it belongs to high-Si and high-K weakly peraluminous calc-alkaline series. The monzogranite is enriched in K, Rb, Th (LILEs) and La, Ce, Sm, Nd(LREEs); and depleted in Ba, U(HREEs) and Ta, Nb(HFSEs). Their zircon $\varepsilon Hf(t)$ values range from 1.21 to 3.46, in response to their two-stage Hf model ages (T_{DM2}) ranging from 1 034 Ma to 1 159 Ma, respectively, indicating that the primary magma was derived from the young crust in Meso-Neoproterozoic. Combined with the regional geological evolution background, it is considered that the Niubiziliang monzogranite formed the closure of North Qaidam ocean, which was the stretching stage product after the collision between Qaidam block and Qilian block.

Key words: monzogranite; zircon U-Pb dating; geochemistry; Hf isotope; tectonic setting; North Qaidam ocean; Niubiziliang

0 Introduction

Since the Phanerozoic, the Qaidam Basin in western China has experienced a complex tectonic evolution, resulting in widely distributed magmatic rocks and related ore deposits. The most widespread rocks are Early Paleozoic magmatic rocks, predominantly granodiorite, tonalite, plagiogranite, monzonitic granite, syenogranite and gabbro. These are the main rock types that comprise the stocks and batholith exposed in Shengligou, Saishenteng Mountain, Tuanyu Mountain, Qaidam Mountain and other areas. Wu *et al.* (2001, 2004) proposed a temporal division of Early Paleozoic magmatic rocks into the late Cambrian-Early-Middle Ordovician subduction type, Late Ordovician collision type, and Late Silurian-Early Devonian tension type. This division suggests that the Early Paleozoic magmatic rocks record a protracted

Received 35 March 2016, accepted 28 April 2016

tectonic evolution.

Compared with the Early Paleozoic magmatic rocks, the Late Paleozoic magmatic rocks are scarce in the studied area. Some work has been done for the Late Devonian and Permian granites, such as the Yematan granite (397 ± 3.6 Ma) (Wu *et al.*, 2004), the Aolaohe tonalite (372 Ma) (Wu *et al.*, 2008), and the Datouyanggou granodiorite (372.0 ± 2.7 Ma) (Wu *et al.*, 2007), but a comprehensive and systematic study of the origin and timing of the Late Devonian magmatism has never been conducted. Particularly in the western part of Northern Qaidam Basin, granites are widespread and exposed together with contemporaneous mafic-ultramafic rocks. Intermediate-acidic intrusive rocks, comprising typical diorite-tonalite-monzolite assemblages, are developed within a number of the Late Devonian intrusions, and they are found in the western part of the studied area between Northern Qaidam Basin and the Altyn fault. The Niubiziliang Cu-Ni ore deposit is the first deposit known to be associated with mafic-ultramafic rocks in Northern Qaidam Basin. The ore-bearing rocks are aged in 373–389 Ma (Devonian). The geology of the ore region is poorly known, especially the origin, precise timing, and evolution of Devonian magmatism. Therefore, monzogranite was selected for analysis in this study. The geochronologcal, geochemical, and Hf isotopic characteristics of monzogranite samples are used to determine their genesis and age of formation in relation to the mafic-ultramafic rocks, to better constrain the tectonic evolution of Northern Qaidam, and the timing of metallogenesis and the geodynamic framework of the Niubiziliang Cu-Ni exploration area during the Late Paleozoic.

1 Geological background

The structural belt that lies within the Northern Qaidam Basin is located on the northeastern margin of the Tibetan Plateau between the Qaidam block and Qilian block. The studied area is located in Niubiziliang, Northwest Qaidam Basin (Fig. 1). The studied outcrops are mainly Jinshuikou swarms within Lower Proterozoic and Quaternary, plus a smaller number of Jurassic, Paleogene and Neogene. The Jinshuikou swarms display a range of lithologies, from biotite-plagioclase gneiss to biotite-garnet-plagioclase gneiss, diopside marble, and occasional quartzite and granulite. The Jurassic strata consist of a combination of sandstone, slate, conglomerate, and argillaceous siltstone. The Paleogene strata comprise a mixture of quartzo-feldspathic sandstone, fine-grained sandstone, pebbly sandstone, sandstone, and fine-grained argillaceous siltstone. The Neogene strata are characterized by mudstone and marl, and the Quaternary strata consist of poorly lithified gravel. A wide-ranging suite of intrusive rocks, such as olivine pyroxenite, pyroxenite, gabbro, basic-ultrabasic rocks, and diorite, monzogranite, and intermediate-acidic rocks, crops out in the studied area (Li, 2011). However, the monzogranite is scarce, occurred only as stocks and dykes (<1 km^2) in the studied area.

2 Sample description and analysis

2.1 Description of samples

Six samples of monzogranite for petrogeochemistry and chronology from different fresh outcrops in Niubiziliang. They are pale white in color, collected at a site (92°4′40E″, 38°45′30″N), with amedium-grained granitic texture and massive structure. It consists of quartz (40%), microcline (30%), plagioclase (25%), biotite (4%), and accessory mineral (1%), mainly including apatite (Fig. 2).

2.2 Sample analysis

2.2.1 Zircon U-Pb dating and Hf isotope analysis

The samples for zircon U-Pb dating were selected and completed in the laboratory of Langfang Regional Geological Survey, Hebei Province by using standard heavy mineral separation technology. Approximately 250 zircons were handpicked from each sample and were embedded within resin discs under a binocular microscope before being polished to expose grain centers. Transmitted and reflected light images were captured using a microscope, and cathodoluminescence (CL) imaging was undertaken using a JEOL scanning

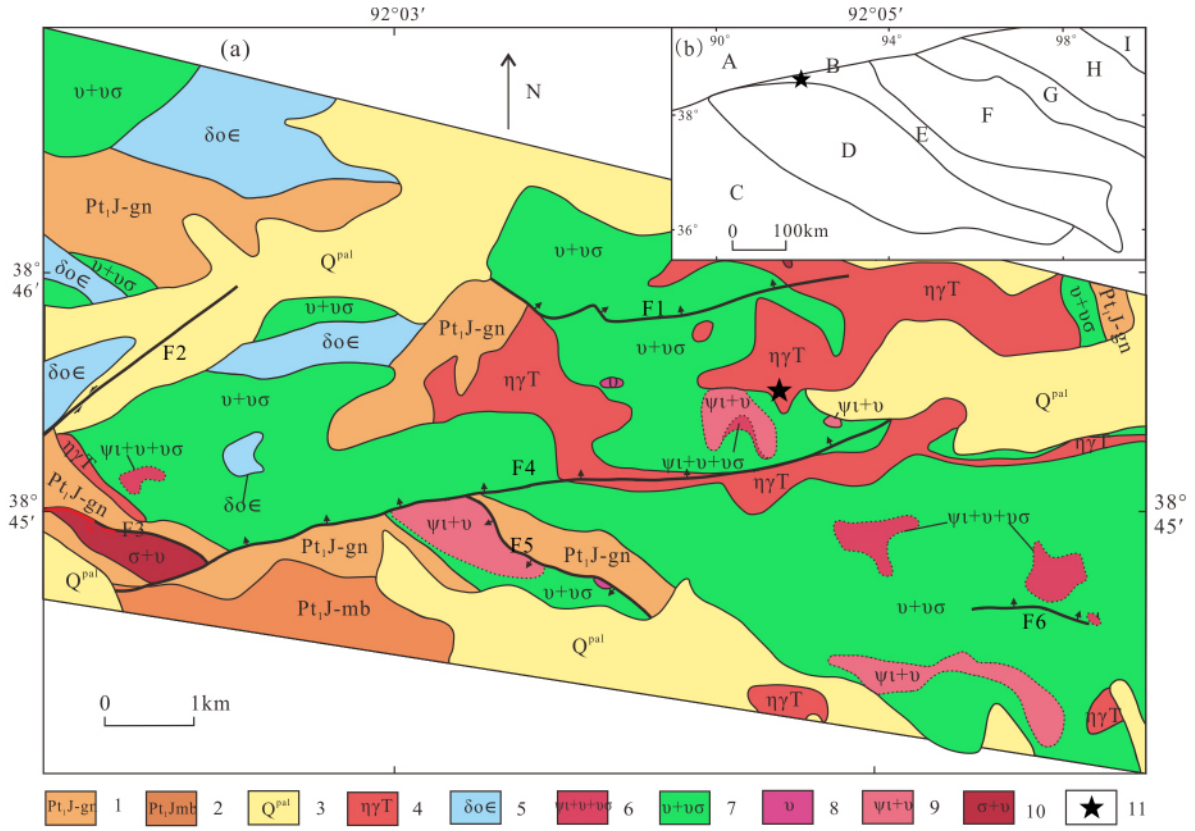

(a) 1. Gneiss in Jinshuikou swarms; 2. marble in Jinshuikou swarms; 3. quaternary; 4. monzogranite; 5. quartz diorite; 6. rhythmic gabbro and olivine websterite; 7. rhythmic gabbro and anorthosite; 8. gabbro; 9. rhythmic gabbro and websterite; 10. rhythmic gabbro; 11. sampling position. (b) A. Tarim ancient land; B. altyn fault; C. east Kunlun orogenic belt; D. Qaidam Basin; E. south Qilian rifting; F. northern Qaidam structural belt; G. middle Qilian block; H. north Qilian continental margin; I. north China continent.

Fig. 1 Geological map of Niubiziliang mining (a) and tectonic location map (b)

electron microscope. Laser ablation (LA)-ICP-MS zircon U-Pb analysis of samples were conducted using an Agilent 7 500 a ICP-MS instrument equipped with a 193 nm laser at the State Key Laboratory of Continental Dynamics, Northwestern University, Xi'an, China, using a 30 μm spot diameter. Details of the analytical technique are described in Yuan *et al* (2004), common Pb concentrations were evaluated following Andersen (2002), and ISOPLOT version 3.0 was used for age calculations and for constructing concordia diagrams (Ludwig, 2003).

In situ zircon Hf isotope analysis was undertaken using a Neptune Plus MC-ICP-MS instrument equipped with a laser ablation at State Key Laboratory of Geological Processes and Mineral Resources, China University of Geosciences (Wuhan), using the instrumental conditions and data acquisition procedures introduced by Hu *et al.* (2012).

2.2.2 Whole-rock geochemistry determination

For geochemical analysis, whole-rock samples, after the removal of altered surfaces, were crushed in an agate mill to 200 mesh. X-ray fluorescence (XRF; PW1401/10) using fused-glass disks and ICP-MS (Agilent 7 500 a with a shield torch) were used to measure the major and trace elements compositions, respectively, at the Testing Center of Jilin University, after acid digestion of samples in Teflon bombs. The analytical results for the BHVO-1, BCR-2, and AGV-1 standards indicate that the analytical precision for major elements and trace elements, which is that the relative deviations are less than 5% when their composition are more than 10 μg/g, otherwise, the rela-

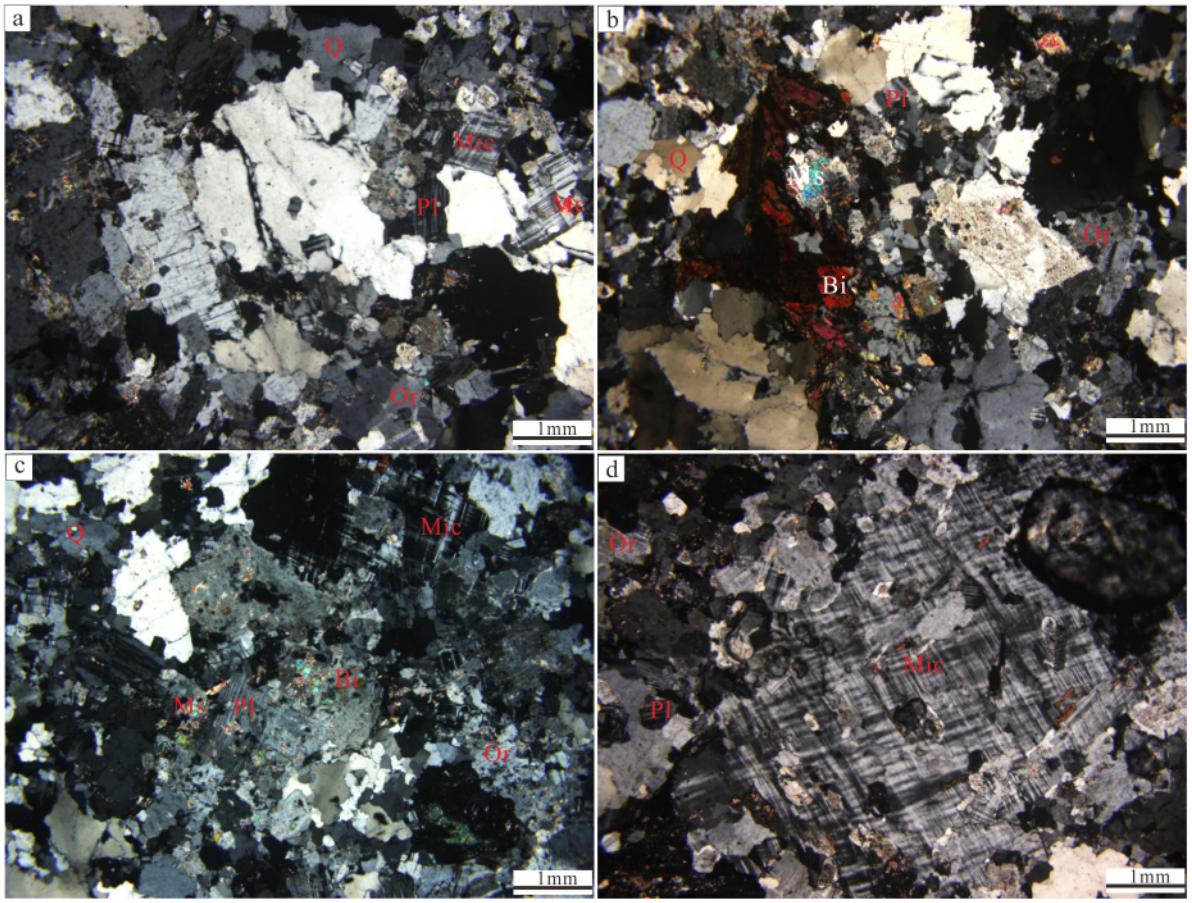

Q-quartz; Or-orthoclase; Bi-biotite; Mic-microcline; Pl-plagioclase; Ms-muscovite

Fig. 2 Photomicrographs of Late Devonian monzogranite in the studied area

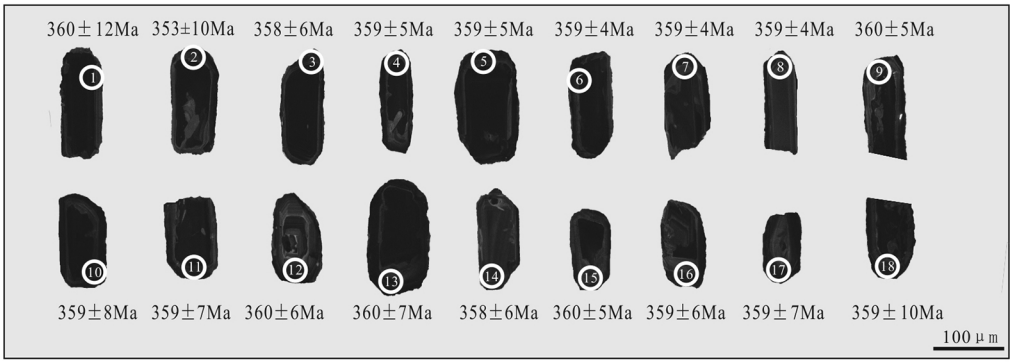

Fig. 3 Cathodoluminescence(CL) images from samples from monzogranite in Niubiziliang

tive deviations are less than 10%.

3 Results

3.1 LA-ICP-MS zircon geochronology

Selected zircons from monzogranite (sample NB-ZL-I-DB-N5) are 100–300 μm long and contain typical magmatic oscillatory zoning (Fig. 3). The results from 18 analytical sites (Table 1) have highly variable Th $(0.481–2.986)\times10^{-3}$ and U $(1.353–9.637)\times10^{-3}$ concentrations, yielding high Th/U

ratios of 0.21 ~ 0.53, all of which is indicative of a magmatic origin for these zircons (Belousova *et al.*, 2002). The $^{206}Pb/^{238}U$ ages of the measuring points are in range of 353–360 Ma, and showing a weighted mean $^{206}Pb/^{238}U$ age of 359.0 ± 2.6 Ma (MSWD = 0.038; Fig. 4a), which is interpreted to be the cry-

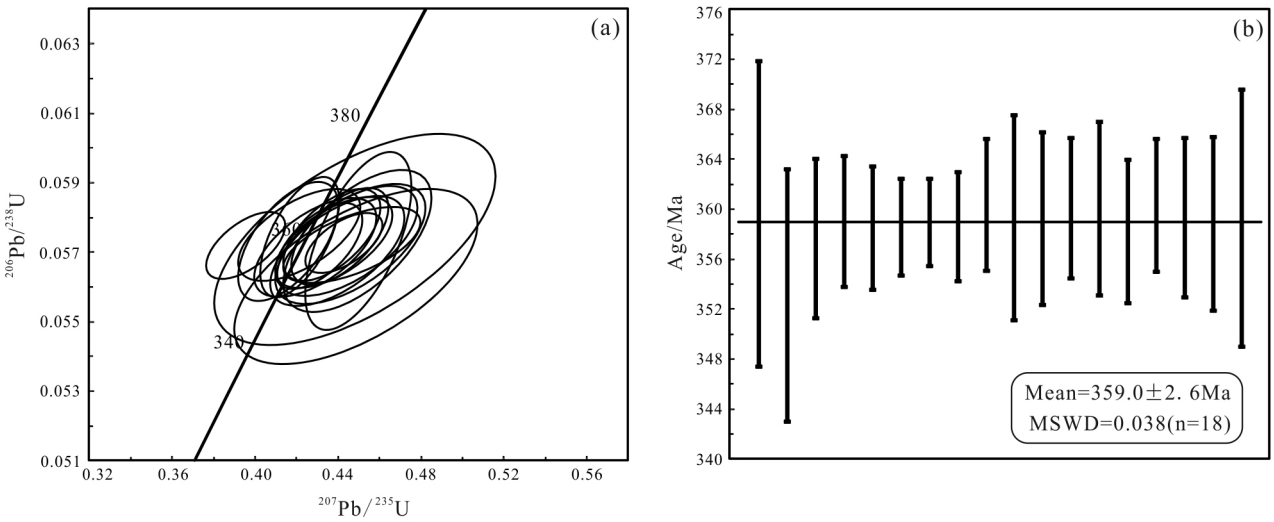

Fig. 4 Concordia diagram (a) and weighted mean ages (b) of zircon U-Pb dating for monzogranite in Niubiziliang

Table 1 LA-ICP-MS U-Pb dating for zircons in Niubiziliang

Samples	Pb /10^{-6}	Th /10^{-6}	U /10^{-6}	Th/U	$^{207}Pb/^{206}Pb$		$^{207}Pb/^{235}U$		$^{206}Pb/^{238}U$		$^{207}Pb/^{206}Pb$		$^{207}Pb/^{235}U$		$^{206}Pb/^{238}U$	
					Ratio	1σ	Ratio	1σ	Ratio	1σ	Age/Ma	1σ	Age/Ma	1σ	Age/Ma	1σ
NBZL-I-DB-N5-01	1073	1954	4601	0.42	0.0525	0.0043	0.4483	0.0448	0.0574	0.0020	309	181	376	31	360	12
NBZL-I-DB-N5-02	538	1225	2330	0.53	0.0539	0.0039	0.4486	0.0387	0.0563	0.0017	365	163	376	27	353	10
NBZL-I-DB-N5-03	986	2014	5258	0.38	0.0536	0.0022	0.4396	0.0213	0.0571	0.0010	354	93	370	15	358	6
NBZL-I-DB-N5-04	284	605	1625	0.37	0.0542	0.0022	0.4379	0.0187	0.0573	0.0009	389	95	369	13	359	5
NBZL-I-DB-N5-05	976	2066	7016	0.29	0.0534	0.0015	0.4307	0.0139	0.0572	0.0008	346	65	364	10	359	5
NBZL-I-DB-N5-06	756	1840	5206	0.35	0.0496	0.0016	0.3954	0.0126	0.0572	0.0006	189	74	338	9	359	4
NBZL-I-DB-N5-07	614	1374	3765	0.37	0.0557	0.0016	0.4428	0.0122	0.0573	0.0006	439	63	372	9	359	4
NBZL-I-DB-N5-08	222	481	1353	0.36	0.0561	0.0028	0.4466	0.0217	0.0572	0.0007	454	109	375	15	359	4
NBZL-I-DB-N5-09	753	1813	4480	0.40	0.0520	0.0023	0.4212	0.0194	0.0575	0.0009	283	100	357	14	360	5
NBZL-I-DB-N5-10	880	1584	6733	0.24	0.0560	0.0027	0.4494	0.0237	0.0573	0.0013	450	107	377	17	359	8
NBZL-I-DB-N5-11	1379	2986	9637	0.31	0.0519	0.0018	0.4161	0.0160	0.0573	0.0011	283	75	353	11	359	7
NBZL-I-DB-N5-12	907	2197	5788	0.38	0.0548	0.0017	0.4409	0.0154	0.0575	0.0009	467	70	371	11	360	6
NBZL-I-DB-N5-13	1090	2574	7626	0.34	0.0529	0.0013	0.4214	0.0127	0.0574	0.0011	324	25	357	9	360	7
NBZL-I-DB-N5-14	311	826	1815	0.46	0.0544	0.0026	0.4292	0.0194	0.0571	0.0009	387	112	363	14	358	6
NBZL-I-DB-N5-15	449	901	4236	0.21	0.0545	0.0018	0.4369	0.0154	0.0575	0.0009	391	72	368	11	360	5
NBZL-I-DB-N5-16	269	648	1841	0.35	0.0571	0.0038	0.4446	0.0223	0.0573	0.0010	494	148	373	16	359	6
NBZL-I-DB-N5-17	230	599	1479	0.40	0.0562	0.0031	0.4460	0.0240	0.0572	0.0011	461	122	374	17	359	7
NBZL-I-DB-N5-18	834	1951	6877	0.28	0.0562	0.0014	0.4497	0.0170	0.0573	0.0017	461	56	377	12	359	10

Table 2 Major(%), REE and trace element content (10^{-6}) and parameter for monzogranite in Niubiziliang

SAMPLE	NBZL-I-DB-B_{5-1}	NBZL-I-DB-B_{5-2}	NBZL-I-DB-B_{5-3}	NBZL-I-DB-B_{5-4}	NBZL-I-DB-B_{5-5}	NBZL-I-DB-B_{5-6}	NBZL-I-DB-B_{5-7}
SiO_2	76.10	75.44	76.11	75.59	74.69	75.11	75.65
TiO_2	0.11	0.16	0.12	0.16	0.14	0.16	0.14
Al_2O_3	12.07	12.81	12.43	12.64	12.70	12.70	12.41
Fe_2O_3	1.01	1.09	0.92	0.78	1.04	0.92	0.93
MnO	0.08	0.08	0.10	0.08	0.09	0.08	0.09
MgO	0.27	0.20	0.18	0.17	0.28	0.23	0.25
CaO	0.68	0.71	0.57	0.94	0.92	0.68	0.62
Na_2O	3.25	3.33	3.13	3.23	3.46	3.36	3.42
K_2O	5.22	4.91	5.22	5.36	5.13	5.35	5.27
P_2O_5	0.02	0.02	0.02	0.02	0.02	0.02	0.02
LOI	0.29	0.44	0.25	0.34	0.35	0.34	0.21
Total	99.68	99.78	99.71	99.89	99.61	99.75	99.83
ALK	8.46	8.24	8.34	8.58	8.59	8.70	8.69
Na_2O/K_2O	0.62	0.68	0.60	0.60	0.67	0.63	0.65
A/CNK	0.99	1.06	1.05	0.98	0.98	1.01	0.99
$Mg^{\#}$	24.20	18.30	17.30	19.00	22.40	19.50	21.20
La	17.10	12.30	17.10	23.70	21.10	20.50	19.30
Ce	33.90	26.30	38.80	50.10	46.20	43.30	39.70
Pr	4.61	3.55	4.03	6.18	6.00	5.54	4.85
Nd	17.60	13.30	14.60	23.70	23.10	21.70	18.60
Sm	4.06	2.86	3.25	5.10	4.91	4.76	4.07
Eu	1.35	1.16	1.24	1.60	1.52	1.48	1.36
Gd	3.79	2.57	3.05	4.94	4.85	4.56	3.80
Tb	0.60	0.41	0.47	0.72	0.74	0.68	0.58
Dy	3.37	2.16	2.46	3.87	4.02	3.70	3.17
Ho	0.69	0.45	0.52	0.78	0.82	0.74	0.63
Er	1.94	1.24	1.43	2.20	2.26	2.03	1.72
Tm	0.29	0.20	0.22	0.31	0.33	0.29	0.25
Yb	1.89	1.06	1.27	1.81	1.96	1.64	1.45
Lu	0.29	0.17	0.22	0.28	0.29	0.24	0.24
Y	15.60	10.10	11.20	17.30	18.00	15.80	13.70
ΣREE	91.50	67.70	88.70	125.20	118.10	111.10	99.80
LREE	78.66	59.42	79.05	110.32	102.85	97.27	87.95
HREE	28.49	18.35	20.82	32.19	33.28	29.68	25.54
LREE/HREE	2.76	3.24	3.80	3.43	3.09	3.28	3.44
La_N/Yb_N	6.49	8.33	9.70	9.41	7.72	8.95	9.58
δEu	1.06	1.30	1.20	0.98	0.95	0.97	1.06
δCe	1.05	1.08	1.05	1.06	1.00	1.04	0.98
Rb	92.11	93.88	108.70	97.86	104.00	94.98	102.00
Ba	400.80	750.80	375.90	1031.00	565.00	772.90	612.10
Th	8.25	9.29	8.06	10.25	10.83	9.49	9.31
U	0.66	0.84	0.57	0.67	0.67	0.64	0.63
Nb	5.91	3.80	4.98	6.29	6.49	5.68	5.65
Ta	0.53	0.35	0.42	0.59	0.60	0.45	0.42
Sr	68.45	91.07	60.50	145.00	111.00	94.00	82.14
Zr	232.00	31.30	120.00	41.40	26.90	36.70	44.70
Hf	3.36	4.69	2.55	2.45	2.55	4.64	2.60
Nb/Ta	9.92	7.16	10.39	10.12	10.98	11.25	8.07
Rb/Sr	1.35	1.03	1.80	0.67	0.94	1.01	1.24
Th/Nb	1.40	2.45	1.62	1.63	1.67	1.67	1.65
La/Nb	9.16	5.82	9.11	5.73	10.48	6.33	8.81

stallization age of the monzogranite.

3.2 Geochemistry characteristics

3.2.1 Major elements

The major and trace element compositions of all the samples are shown in Table 2. $w(SiO_2)$ is 74.69%–76.11%, $w(Al_2O_3)$ is 12.07%–12.81%, $w(Na_2O + K_2O)$ is 8.24%–8.70%, $Mg^{\#}$ values of 17.3–24.2, Na_2O/K_2O ratios of 0.60–0.68, and A/CNK values of 0.98–1.06. They are classified as granite in a total alkali versus SiO_2 (TAS) diagram (Fig. 5), and are classified as the feature of weakly peraluminous rock (Fig. 6a) and high-Si, high-K and calc-alkaline in a K_2O versus SiO_2 diagram (Fig. 6b).

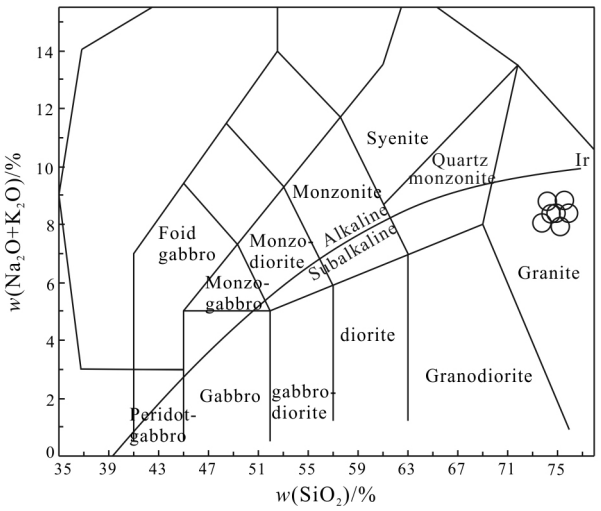

Fig. 5 TAS diagram of igneous rock

3.2.2 Trace elements

The monzogranite in the studied area has chondrite-normalized rare earth element (REE) patterns that is characterized by light REE (LREE = (59.42 × 10^{-6}–110.32 × 10^{-6}) enrichments and heavy REE (HREE = (18.35–33.28) × 10^{-6} depletions (Fig. 7a), as well as $(La/Yb)_N$ values of 6.49–9.70 and minor Eu anomalies ((Eu = 0.95–1.30). These samples also have primitive-mantle-normalized trace element variation patterns that are enriched in large ion lithophile elements (LILEs; e.g., Rb and K) and light rare earth elements (LREES; e.g., La, Ce, Sm and Nd), as well as strongly depleted in the high field strength elements (HFSEs; e.g., Ti, Nb, Ta and Th) and incompatible elements (Ba, U and Sr) (Fig. 7b).

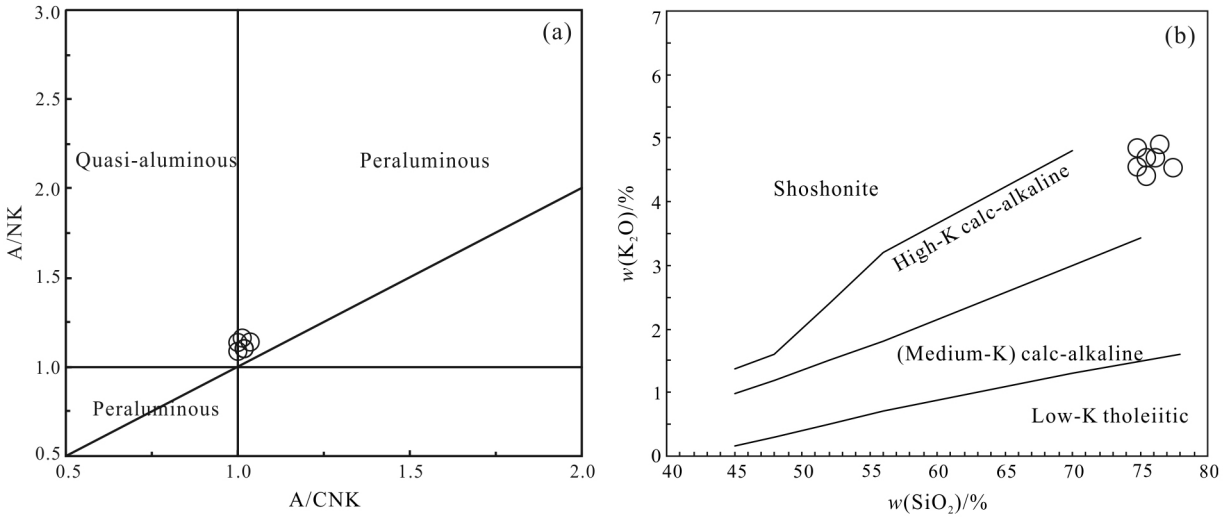

Fig. 6 A/CNK-A/NK diagram (a) and SiO_2 versus K_2O diagram (b) for monzogranite

3.3 Lu-Hf isotope

Nine zircons of the monzogranite have $^{176}Lu/^{177}Hf$ ratios between 1.14×10^{-3} and 1.487×10^{-3} (Table 3), which indicates a lower radiogenic Hf accumulation in the long evolution after the rock formation. Thus we choose $^{176}Hf/^{177}Hf$ ratio to discuss the information of petrogenesis (Wu *et al.*, 2007). The $F_{Lu/Hf}$ value (−0.925 67 to −0.965 65) is less than the $^{176}Hf/^{177}Hf$ value of the mafic crust (0.34) (Amelin

et al., 2000) and the salic crust (−0.72) (Vervoort *et al.*, 1996) for all analytical sites, and their two-stage Hf model ages (T_{DM2}) fall between 1 034 Ma and 1 059 Ma.

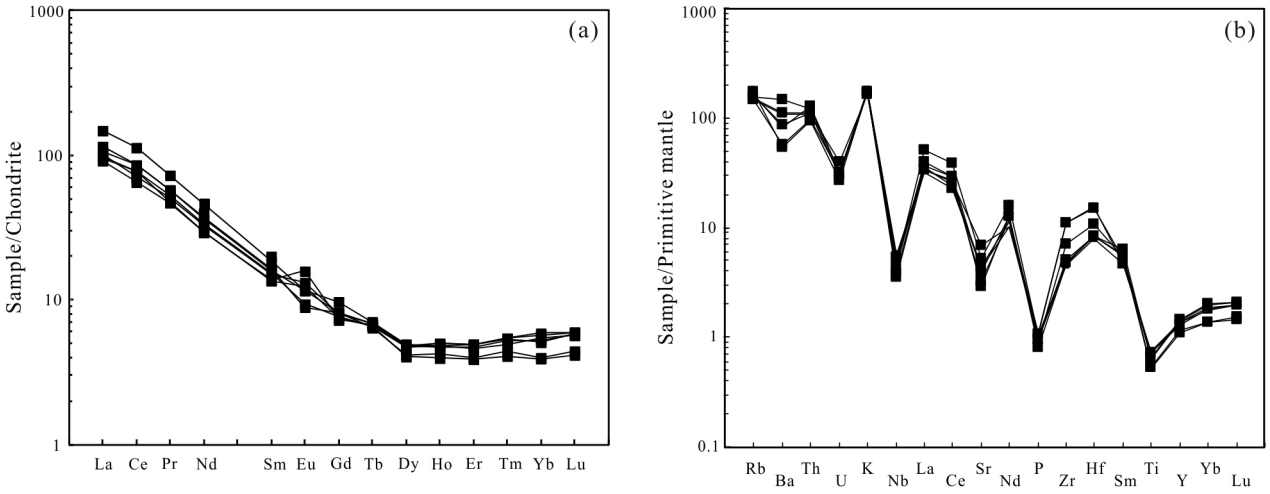

Fig. 7 Chondrite-normalized REE distribution pattern (a) and primitive mantle-normalized trace element spider diagram (b) for monzogranite

Table 3 Hf isotope composition of zircon for Niubiziliang monzogranite

Testing point	t(Ma)	$^{176}Yb/^{177}Hf$	$^{176}Lu/^{177}Hf$	$^{176}Hf/^{177}Hf$	1σ	εHf(t)	TDM1(Hf)	TDM2(Hf)	fLu/Hf
NBZL-1-DB-N5-1	350	0.031281	0.001140	0.282654	0.001788	3.26	850.14	1045.04	−0.97
NBZL-1-DB-N5-2	350	0.033472	0.001241	0.282625	0.000277	2.21	893.57	1103.35	−0.96
NBZL-1-DB-N5-3	350	0.037211	0.001382	0.282620	0.000345	2.00	904.15	1115.12	−0.96
NBZL-1-DB-N5-4	350	0.036263	0.001307	0.282661	0.000340	3.46	844.26	1033.82	−0.96
NBZL-1-DB-N5-5	350	0.032720	0.001226	0.282658	0.000691	3.38	846.61	1038.55	−0.96
NBZL-1-DB-N5-6	350	0.037574	0.001382	0.282612	0.000268	1.71	915.83	1131.26	−0.96
NBZL-1-DB-N5-7	350	0.035213	0.001333	0.282638	0.000217	2.64	877.53	1079.33	−0.96
NBZL-1-DB-N5-8	350	0.067761	0.002468	0.282630	0.000555	2.11	916.10	1108.77	−0.93
NBZL-1-DB-N5-9	350	0.041452	0.001487	0.282598	0.001016	1.21	937.46	1158.81	−0.96

4 Discussion

4.1 Character of rock source area

Geochemically, the monzogranite is characterized by high SiO_2 and K_2O contents, low MgO contents, and Al_2O_3 values between 12.07 and 12.81. Thus, they belong to the high-K weakly peraluminous calc-alkaline granite series. Their Mg, Co, Ni, and Cr contents are consistent with lithospheric values. $Mg^{\#}$ values range from 17.3 to 24.2, and Nb/Ta values (7.16–11.25) are similar to those of crustal magma (Weyer *et al.*, 2003); the Th/Nb values (1.40–2.45) are also higher than the average for continental crust (Saunders *et al.*, 1988; Weaver, 1991). Thus, it is concluded that the monzogranite originated from the deep crust.

The residual phase of the granite source is characterized by the presence of Sr and Yb (Defant & Drummond, 1990; Defant *et al.*, 2002). Sr resides within plagioclase, while Yb resides within garnet and amphibole (Zhang *et al.*, 2004). The monzogranite itself has low Sr (60.5×10^{-6}–145.0×10^{-6}) and Yb (1.06×10^{-6}–1.96×10^{-6}) contents, and a weak negative Eu anomaly, indicating that the residual phase

contains plagioclase, garnet, and amphibole.

The $\varepsilon Hf(t)$ values of magmatic zircon range from 1.21 to 3.46, falling between the chondrite evolution line and the depleted mantle evolution line (Fig. 8). The narrow range of Hf isotope compositions indicates a uniform magma source (Amelin *et al.*, 1999; Griffin *et al.*, 2002). These results, combined with the Hf model age, indicate that the monzogranite was produced by partial melting of juvenile Mesoproterozoic lower crust.

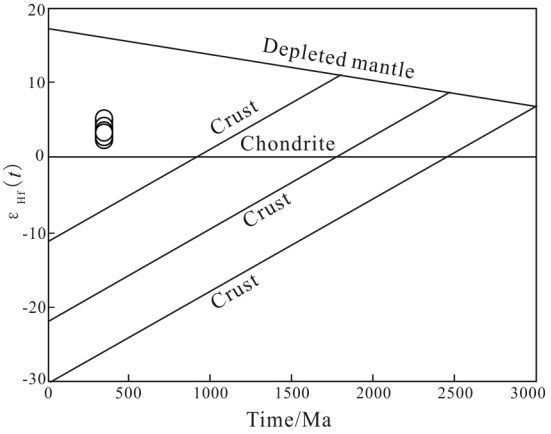

Fig. 8 Hf isotopic compositions of the Monzogranite

4.2 Tectonic setting

The monzogranite examined in this study is of the high-Si and high-K weakly peraluminous calc-alkaline series, with low contents of alkali feldspar at Niubiziliang, indicating an orogenic granitoid (Maniar & Piccoli, 1989). The monzogranite has $Na_2O + K_2O = (8.24-8.70) \times 10^{-6}$, $Na_2O/K_2O = 0.60-0.68$, $Nb = (3.80-6.49) \times 10^{-6}$, $Ta = (0.35-0.60) \times 10^{-6}$, $Zr = (26.9-232) \times 10^{-6}$, and $Hf = (2.45-4.69) \times 10^{-6}$ (Jiang *et al.*, 2015). In addition, they are enriched in large ion lithophile elements and depleted in high field-strength elements. These properties indicate that they formed in a post-orogenic extensional environment (Fig. 9).

The studied area is a structural belt located between the Qaidam block and Qilian block in Niubiziliang, in the western segment of Northern Qaidam Basin. The belt contains extensive mafic-ultramafic bodies along its length, and the zircon U-Pb age of gabbro (367.0 Ma) (Ling *et al.*, 2014) at Niubiziliang is within error of the age of monzogranite (359.0 Ma) in the studied area, suggesting a typical bimodal volcanic rock association and implying an extensional

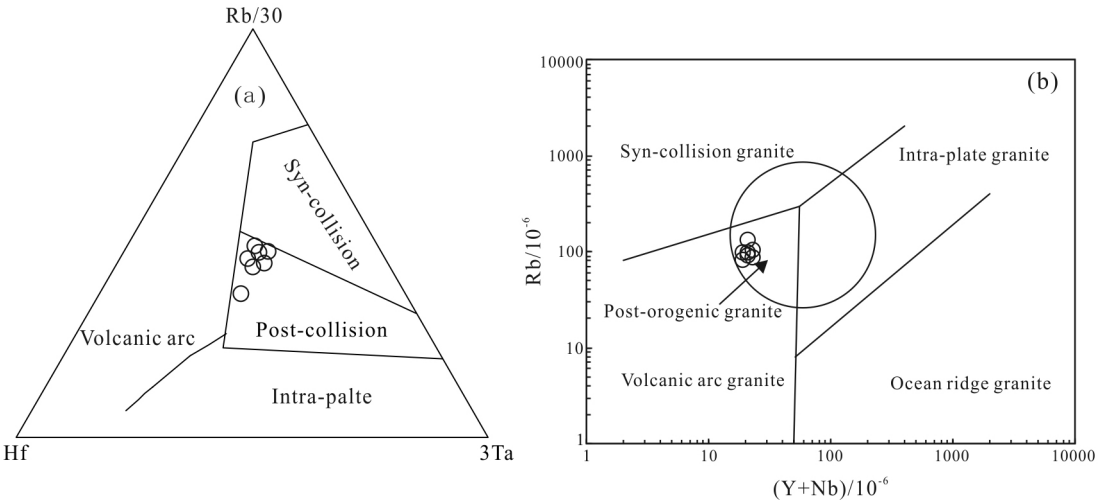

Fig. 9 Diagrams of Hf-Rb/30-3Ta (a) and (Y + Nb)-Rb (b) for monzogranite

environment in the Late Devonian.

Previous studies have focused on the Early Paleozoic tectonic evolution of Northern Qaidam Basin. Song *et al.* (2009) proposed that Early Paleozoic orogenesis in the region could be divided into two stages. First, an oceanic-crust subduction stage occurred, during which the North Qaidam ocean, located between the Qaidam block and Qilian block, was sub-

ducted during the Early Paleozoic. This resulted in the formation of the Wanggaxiu gabbro complex (468–522 Ma) (Zhu *et al.*, 2010) in the Dulan area, the arc magmatite (514 Ma) of the Tanjianshan Group (Zhao *et al.*, 2003), and the adakitic dacite (514 Ma) at Jilvsu (Shi *et al.*, 2003). Subduction continued into the Late Ordovician, creating the Shaliuhe ophiolite assemblage, which contains a metamorphosed coesite-bearing gabbro (450 Ma) (Zhang *et al.*, 2009). The second stage involved continental collision, due to the subduction of the North Qaidam oceanic plate. This resulted in a series of continental subduction-collision assemblages, such as the Yukahe eclogites and gneiss (423-448 Ma) (Chen *et al.*, 2007), the large porphyritic granite (446 ± 7.7 Ma) at Qaidamshan (Wu *et al.*, 2001), and the Tataleng rapakivi granite (441 Ma) (Shen *et al.*, 2007). At the same time, the collision between the Qaidam block and Qilian block resulted in crustal thickening and the generation of the adakitic Tieshiguan granite (422.0 ± 6.4Ma) (Zhou *et al.*, 2014). At the time of formation of dense eclogite, delamination of the lithospheric mantle and asthenospheric upwelling resulted in recycling of the subducted slab. This led to the formation of the Yematan granite (397 Ma) (Wu *et al.*, 2004) and the mylonitized gneiss (402 ± 1 Ma) at Dulan (Song *et al.*, 2005). These observations, combined with the formation of Devonian molasse (Qian *et al.*, 2015) in Northern Qaidam Basin, indicate that the monzogranite formed in a post-orogenic extensional environment. Therefore, the Late Devonian tectonic setting of the Niubiziliang area was an ocean-continent collision zone, which resulted in crustal thickening, delamination of lithospheric mantle, asthenospheric upwelling, orogenic stretching and collapse, and subsequent crustal thinning between the Qaidam block and Qilian block after the closure of the North Qaidam ocean, which resulted in partial melting of the lower crust and the formation of a bimodal volcanic rock assemblage.

5 Conclusions

(1) The LA-ICP-MS U-Pb weighted average age of monzogranite in Niubiziliang area was 359.0 ± 2.6 Ma, MSWD = 0.038. The results indicate the rock formed in Late Devonian.

(2) The primitive magma of the monzogranite originated from the partial melting of juvenile crust in Mesoproterozoic, it belongs to I-type granite.

(3) The monzogranite formed in a post-orogenic extensional environment between the Qaidam block and Qilian block after the closure of the North Qaidam ocean.

References

Amelin Y, Lee D C, Halliday A N, *et al*. 1999. Nature of the Earth's earliest crust from hafnium isotopes in single detrital zircons. *Nature*, **399**: 252-255.

Amelin Y, Lee D C, Halliday A N. 2000. Early-Middle Archean crustal evolution deduced from Lu-Hf and U-Pb isotope studies of single zircon grains. *Geochimica et Cosmochimica Acta*, **64**(24): 4205-4225.

Anderson T. 2002. Correction of common lead in U-Pb analyses that do not report ^{204}Pb. *Chemical Geology*, **192**(1/2): 59-79.

Belousova E, Griffin W, Reilly S Y O, *et al*. 2002. Igneous zircon: trace element composition as an indicator of source rock type. *Contributions to Mineralogy & Petrology*, **143**(5): 602-622.

Chen D L, Sun Y, Liu L, *et al*. 2007. The metamorphic ages of the Yukahe eclogites in the North Qaidam: zircon LA-ICP-MS in-situ dating. *Science in China* (*Ser. D*): *Earth Sciences*, **37**(Suppl.): 279-287.

Defant M J, Drummond M S. 1990. Derivation of some modern arc magmas by melting of young subducted lithosphere. *Nature*, **374**: 662-665.

Defant M J, Xu J F, Kepezhinskas P, *et al*. 2002. Adakites: some variations on a theme. *Acta Petrologica Sinica*, **18**: 129-142.

Griffin W L, Wang X, Jackson S E, *et al*. 2002. Zircon chemistry and magma mixing, SE China: in-situ analysis of Hf isotopes, Tonglu and Pingtan igneous complexes. *Lithos*, **61**(3/4): 237-269.

Hu Z C, Liu Y S, Gao S, *et al*. 2012. Improved in situ Hf isotope ratio analysis of zircon using newly designed X skimmer cone and in combination with the addition of nitrogen by laser ablation multiple collector ICP-MS. *Journal of Analytical Atomic Spectrometry*, **27**(9): 1391-1399.

Jiang S, Wu W Z. 2015. A rough features and causes analysis in high field strength elements aspect for post-orogenic

granite. *Shandong Industrial Technology Magazine*, **16** (19): 209-210.

Li S J. 2011. Geodynamic evolution of Qilian orogenic belt and metallogenesis of endogenous metals: doctor's degree thesis. Changchun: Jilin University.

Ling J L, Zhao Y F, Kang Z, *et al*. 2014. Petrogenesis and mineralization of Niubiziliang mafic-ultramafic intrusion in the northern margin of Qaidam Block, NW China. *Acta Geologica Sinica*, **30**(6): 1628-1646.

Ludwig K R. 2003. User's manual for Isoplot 3.00: a geochronological toolkit for Microsoft Excel. [s. l]: Berkeley Geochronology Center Special Publication, 74.

Maniar P D, Piccoli P M. 1989. Tectonic discrimination of granitoids. *Geological Society of America Bulletin*, **101** (5): 635-643.

Qian B, Zhang Z M, Zhang Z B, *et al*. 2015. Ziron U-Pb geochronology of Niubiziliang mafic-ultramafic intrusion on the northwest margin of Qaidam Basin, Qinghai. *Geology in China*, **42**(3): 482-493.

Saunders A D, Norry M J, Tarney J. 1988. Origin of MORB and chemically depleted mantle reservoirs: trace element constraints. *Journal of Petrology*, Special Volume(1): 425-445.

Shen W H. 2007. The features and genesis of Tataleng rapakivi granite in North Qaidam Basin: master's degree thesis. Xi'an: Chang'an University.

Shi R D, Yang J S, Wu C L. 2003. The discovery of adakitic dacite in Early Palaeozoic island arc volcanic rocks on the northern margin of Qaidam Basin and its geological significance. *Acta Petrogical et Mineralogical*, **22**(3): 229-237.

Song S G, Niu Y L, Zhang L F, *et al*. 2009. Time constraints on orogenesis from oceanic subduction to continental subduction, collision, and exhumation: an example from North Qilian and North Qaidam HP-UHP belts. *Acta Geologica Sinica*, **25**(9): 2067-2077.

Song S G, Zhang L F, Chen J. 2005. Sodic amphibole exsolutions in garnet-perdotite, North Qaidam UHPM belt, NW China: implications for ultra deep-origin and hydroxyl defects in mantle garnets. *American Mineralogist*, **90**: 814-820.

Vervoort J D, Patcett P J, Gehrels G E, *et al*. 1996. Constraints on early earth differentiation from hafnium and neodymium isotopes. *Nature*, **379**: 624-627.

Weaver B L. 1991. The origin of ocean island basalt end-member compositions: trace element and isotopic constraints. *Earth and Planetary Science Letters*, **104**(2/4): 381-397.

Weyer S, Munker C, Mezger K, *et al*. 2003. Nb/Ta, Zr/Hf and REE in the depleted mantle: implications for the differentiation history of the crust-mantle system. *Earth & Planetary Science Letters*, **3**(3/4): 309-324.

Wu C L, Gao Y H, Wu S P, *et al*. 2007. Zircon SHRIMP dating of Paleozoic granite in Da Qaidam of the Northern Qaidam Basin. *Acta Geologica Sinica*, **23**(8): 1861-1875.

Wu C L, Gao Y H, Wu S P, *et al*. 2008. Zircon SHRIMP U-Pb dating and lithogeochemistry of granite in western Qaidam. *Science in China* (*Ser. D*): *Earth Sciences*, **38**(8): 930-949.

Wu C L, Yang J S, Li H B, *et al*. 2001. Zircon SHRIMP dating of granite in Qaidam Mountain. *Science Bulletin*, **46** (20): 1743-1747.

Wu C L, Yang J S, Wooden J L, *et al*. 2004. Zircon SHRIMP dating of granite in Dulan on the north margin of the Qaidam Basin. *Chinese Science Bulletin*, **49**(16): 1667-1672.

Wu C L, Yang J S, Xu Z Q, *et al*. 2004. The effect of granitic magmatism in Paleozoic UHPM belt of Northern Qaidam Basin. *Acta Geologica Sinica*, **78**(5): 658-674.

Wu F Y, Li X H, Zheng Y F, *et al*. 2007. Lu-Hf isotopic system and petrology applications. *Acta Geological Sinica*, **23** (2): 185-220.

Yuan H L, Gao S, Liu X M, *et al*. 2004. Accurate U-Pb age and trace element determinations of zircon by laser ablation-inductively coupled plasma-mass spectrometry. *Geostandards and Geoanalytical Research*, **28**(3): 353-370.

Zhang G B, Zhang L F, Song S G. 2009. UHP metamorphic evolution and SHRIMP geochronology of a meta-ophiolitic gabbro in the North Qaidam. NW China. *Journal of Asian Earth Sciences*, **35**(3): 310-322.

Zhang Q, Li C D, Miao L C, *et al*. 2004. High Sr low Y and low Sr high Y of Mesozoic granite in Hebei: geochemistry, causes and its relationship with mineralization. *Acta Geologica Sinica*, **20**(2): 269-284.

Zhao F Q, Guo J J, Li H K, *et al*. 2003. Geological characteristics and the isotope chronology of Tanjianshan Group in Xitieshan area, North Qaidam. *Journal of Mineralogy and Petrology*, **22**(1): 28-31.

Zhou B, Zheng Y Y, Tong H K, *et al*. 2014. Zircon dating of Early Paleozoic adakitic granite on the northern margin of Qaidam Basin and its geological significance. *Geoscience*, **28**(5): 875-883.

Zhu X H, Chen D L, Liu L, *et al*. 2010. Zircon LA-ICP-MS U-Pb dating of the Wanggaxiu gabbro complex in the Dulan area, northern margin of Qaidam Basin, China and its geological significance. *Geological Bulletin of China*, **29** (2/3): 227-236.